Dynamic Forcing and Mesoscale Variability of Heavy Precipitation Events over the Sierra Nevada Mountains

HEATHER DAWN REEVES AND YUH-LANG LIN

North Carolina State University, Raleigh, North Carolina

RICHARD ROTUNNO

National Center for Atmospheric Research, Boulder, Colorado

(Manuscript received 2 February 2007, in final form 13 April 2007)

ABSTRACT

The aim of this research is to investigate the causes for an isolated maximum in precipitation that is typically found along the northern half of the Sierra Nevada mountains of California, in the vicinity of Plumas National Forest (PNF), during moderate to heavy precipitation events. Particular attention was paid to the role various mesoscale (i.e., <200 km) terrain features may have played in localizing the precipitation at PNF. Numerical simulations and sensitivity experiments for two cases of heavy precipitation at PNF reveal that the extent to which terrain acts to focus precipitation is case sensitive. In the first case, the upstream flow was characterized by a strong horizontal gradient in wind speed and moisture. This gradient led to differential deflection of airstreams incident to the range and, consequently, localized convergence and enhanced rain rates at PNF. This localized enhancement occurred regardless of whether any terrain variations were present in the simulations or not. The second case was characterized by more a horizontally uniform upstream flow and showed a much stronger sensitivity to terrain variations, in particular, short- and long-wavelength undulations along the leading (west) edge of the Sierra Nevada range. When these undulations were removed, no localized maxima in precipitation occurred.

1. Introduction

Northern California is well known for heavy precipitation that can lead to flooding in central California during winter storms or later in the season as frozen precipitation at higher elevations melts (Dettinger et al. 2004). Climatological studies reveal there exists a distinct mesoscale variability in the average precipitation distribution for California with an isolated maximum near Plumas National Forest (PNF; Fig. 1a). This maximum spans the Whitmore, Feather River, Yuba River, Bear River, Butte Creek, and Eastern Tehama watersheds. An understanding of the underlying dynamical causes for this maximum is important because rainfall runoff from these watersheds ultimately drains into the Sacramento River, which flows through Sacramento, a city with a rather high flood threat and large population. The causes for the precipitation maximum at PNF are explored in this paper. As will be demonstrated, dynamical causes are case dependent, but two important forcings have been identified: 1) convergence associated with upstream horizontal gradients in moisture and wind speed and 2) enhancement associated with mesoscale (i.e., <200 km) terrain features.

Figure 1a shows the average annual precipitation from 1961 to 1990 for California according to the U.S. Geological Survey (USGS) rain gauge data. During this sampling period, more precipitation, on average, fell over the northern half of the mountain complex than over the southern half. Within this larger shield of enhanced precipitation are three maxima with values in excess of 1270 mm: these are labeled as CR, MS, and PNF due to their relative proximities to the Coastal Range, Mount Shasta, and Plumas National Forest.

Corresponding author address: Heather Dawn Reeves, NCAR, P.O. Box 3000, Boulder, CO 80307-3000.
E-mail: heather.reeves@applemail.org

DOI: 10.1175/2007MWR2164.1

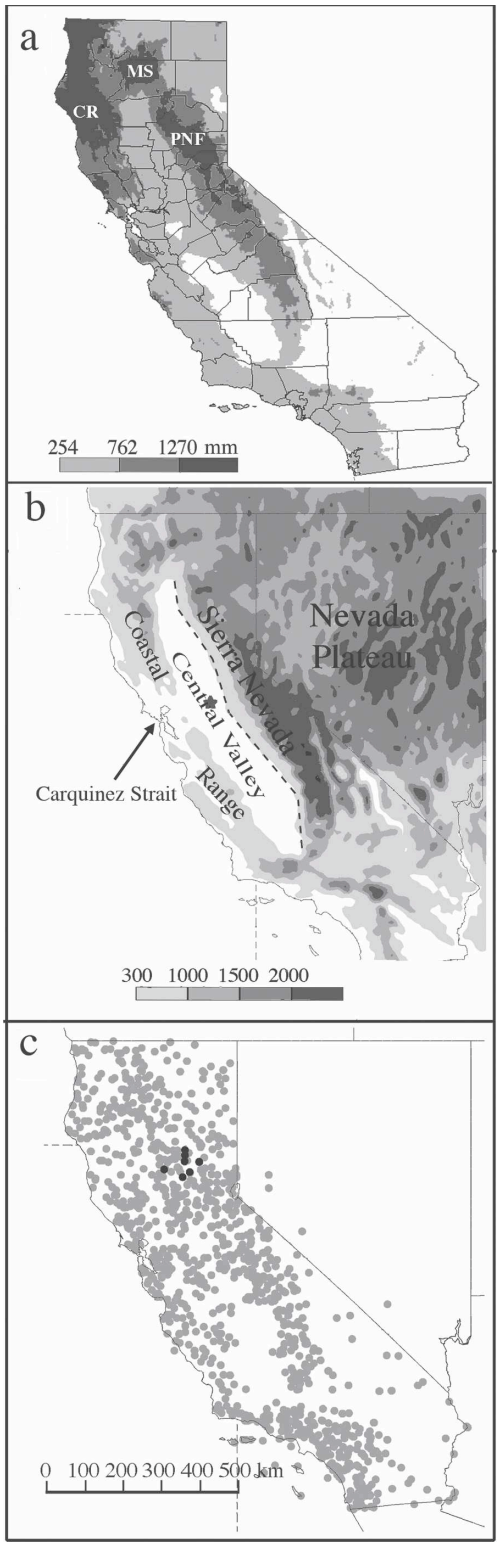

FIG. 1. (a) Average annual precipitation from 1961–1990 (from USGS). The approximate locations of the Coastal Range (CR), Mount Shasta (MS), and Plumas National Forest (PNF) are given. (b) The terrain of the southwestern United States (shaded, m). The dashed line denotes the leading edge of the Sierra Nevada mountains. The star denotes the location of the Sloughhouse wind profiler. (c) Locations of rain gauge observations; those stations shaded black were used for determining hourly rain rate for the profiled cases. Those stations are the Jordan, Bangor, Fourtrees, Brush Creek Ranger Station, Forbestown, Pike, Bucks Creek, and La Porte rain gauges.

(We note that the individual maxima labeled MS and PNF cover a larger aerial extent than do Mount Shasta and the Plumas National Forest; these names are simply chosen for convenience.) A similar mesoscale distribution appears in investigations of smaller or different time series, or even for individual events (Gershunov et al. 2000; Kim et al. 2000; Pandey et al. 2000; Leung and Qian 2003; Ralph et al. 2004; Galewsky and Sobel 2005; Mo et al. 2005, Yuan et al. 2005). Causal factors leading to enhanced precipitation at CR and MS have been explored in numerous journal articles (Miller and Kim 1996; Yu and Smull 2000; Colle et al. 2002; White et al. 2003; Ralph et al. 2004; Neiman et al. 2004; James and Houze 2005; Persson et al. 2005; Kingsmill et al. 2006) and, in general, attribute enhanced precipitation to the forced vertical ascent of moist prefrontal air and/or a barrier jet over the orographic obstructions local to these regions.

A perusal of the literature shows that enhanced precipitation at PNF may occur for a variety of synoptic-scale flows (Heggli and Reynolds 1985; Heggli and Rauber 1988; Mitchell and Blier 1997; Dettinger et al. 2004). Heggli and Rauber (1988) identified 5 synoptic regimes based on a sampling of 63 storms that affected California from the 1983/84 to the 1986/87 seasons. Type I cases are described as having a developing storm in strong westerly or southwesterly flow and having heavy, sustained precipitation. Type II cases are described as having a moderate amplitude shortwave trough that is associated with an occluded storm. Type III cases are characterized by split flow in the midtroposphere associated with a dissipating storm. The type IV regime is characterized by a cutoff low or large-amplitude shortwave near 40°N. The final category, type V, is described as having a large-amplitude longwave pattern producing cold, northerly storms. Types I, II, and III have predominantly zonal basic-state flow while Types IV and V have predominantly meridional basic state flow.

Because the synoptic flow patterns may vary widely, a logical expectation is that terrain features particular to California may act to enhance rain rates at PNF. The primary topographic feature in California is the Sierra Nevada range, which has an average half-width of about 100 km (Fig. 1b). The Sierra Nevada range rep-

resents the leading edge of the Nevada Plateau, which has an average height of about 1600 m. There are numerous transverse peaks along the range that represent a short-wavelength undulation along its crest. However, there is also a long-wavelength, north–south to northwest–southeast undulation at lower elevations; this "zig-zagging" is highlighted by the dashed line in Fig. 1b. The secondary range in California is the Coastal Range, which is located along the California coast and is separated from the Sierra Nevada mountains by the approximately 200-km-wide Central Valley. The Coastal Range is marked by a gap at San Francisco, California, known as the Carquinez Strait. The effect of these terrain variations on precipitation has not been directly addressed with respect to PNF. However, numerous investigators have observed that enhanced precipitation at PNF often occurs in conjunction with southerly barrier jet formation along the western face of the Sierra Nevada mountains (Parish 1982; Marwitz 1983, 1987; Reynolds and Kuciauskas 1988; Meyers and Cotton 1992; Rauber 1992; Galewsky and Sobel 2005). It is possible that rain rates are enhanced at PNF because it is at this location that the barrier jet encounters the slope at a more perpendicular angle. The aim of this paper is to understand the mechanisms for enhanced precipitation at PNF through consideration of two case studies.

This paper is organized as follows: in section 2, two observed cases of heavy precipitation along the Sierra Nevada mountains are presented (30–31 December 2005 and 27–28 February 2006). Numerical simulations and sensitivity tests of the cases are discussed in sections 3 and 4. Finally, conclusions are presented in section 5.

2. Observations from two heavy precipitation events

Unless otherwise noted, all analyses from the individual cases were performed using the North American Regional Reanalysis dataset (NARR; Mesinger et al. 2006), which ingests the initial conditions from the North American Mesoscale Model (NAM; Rogers et al. 1995) forecasts as well as observed precipitation and surface measurements and has a grid spacing of 32 km and a temporal resolution of 3 h. Analyses from this dataset were compared to observed quantities including rain gauge measurements, surface winds, sea level pressure, satellite-derived water vapor, etc., to make sure NARR adequately captured the events. The agreement between these comparisons (not shown) was good.

The 30–31 December case fell into the type I category of Heggli and Rauber (1988). The 300-hPa winds and heights (Fig. 2a) indicate that the upper-level flow incident to and over California was predominantly westerly with weak ridging over the western United States and was in the early stages of cyclonic development. At 850 hPa (Fig. 2c), the flow immediately upstream of California was also more-or-less westerly. Embedded in this flow was a low-level jet with average wind speeds between 20 and 28 m s^{-1}. This jet advected relatively moist air with mixing ratio (q) values between 6 and 9 g kg^{-1} over California. The flow patterns in Fig. 2c are consistent with the "classic" atmospheric-river cases described in Ralph et al. (2004, 2005) and Kingsmill et al. (2006). The storm total precipitation distribution for the 30–31 December case is shown in Fig. 2e.[1] Note that there were localized maxima along the Coastal Range and at PNF. The 27–28 February event was a type IV case (Heggli and Rauber 1988). This case had a shortwave trough located over the eastern Pacific Ocean (Fig. 2b) with a cutoff low pressure center just west of the California–Oregon coast. Flow over and incident to California was from the southwest. At 850 hPa (Fig. 2d), there was a well-defined north–south-oriented baroclinic zone (indicated by the cold front symbol) and the airstreams incident to California were southerly from the prefrontal region of the baroclinic system. Average mixing ratios at 850 hPa in the moist tongue of the prefrontal region were between 7 and 8 g kg^{-1}. The storm total precipitation (Fig. 2f) had enhanced accumulations along the west slope of the Sierra Nevada mountains with the greatest accumulations at PNF.

A time sequence of hourly rain gauge measurements from the December and February cases is shown in Figs. 3a,b, respectively.[2] The episode of moderate to heavy precipitation (i.e., the time period over which rain rates consistently exceeded 2.08 mm h^{-1}, or 50 mm day^{-1}) for the December case lasted 22 h from 2200 UTC 30 December to 1800 UTC 31 December with a maximum rain rate of 13 mm h^{-1} at 0800 UTC 31 December. There were several secondary maxima, the largest of which (11.9 mm h^{-1}) occurred at 1600 UTC 31 December. The accumulated precipitation for this time period and these stations was 224 mm. The rain rate for the February case shows precipitation accumulations in excess of 2.08 mm h^{-1} started at 0500 UTC 27 February and ended at about 0000 UTC 28 February.

[1] In Figs. 2e,f, the beginning (ending) of a storm is defined as that time when hourly accumulations at PNF exceeded (did not exceed) 2.08 mm h^{-1}.

[2] Only stations in the vicinity of PNF (shaded black in Fig. 1c) reporting hourly accumulations were used in this and other similar analyses.

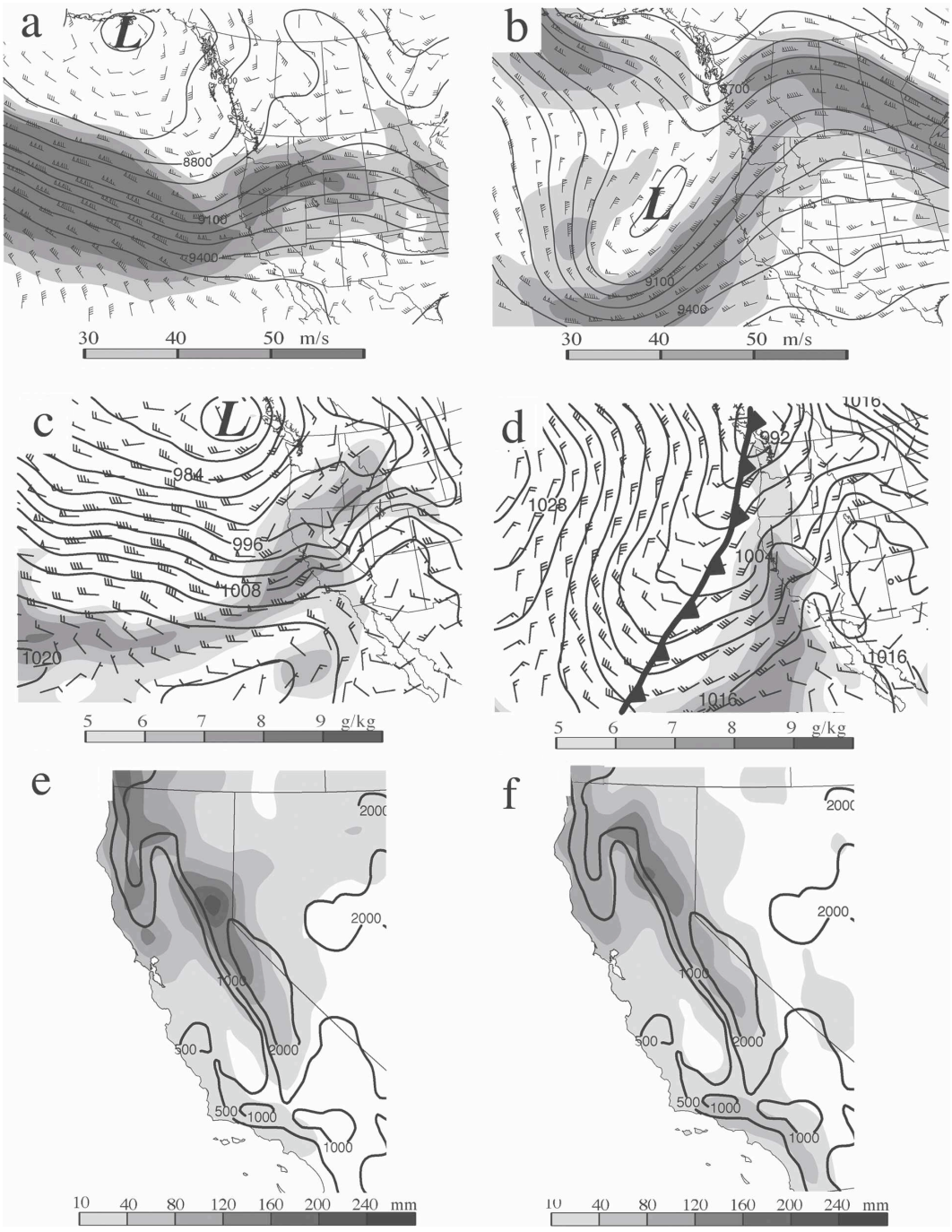

FIG. 2. The 300-hPa wind speeds (shaded as in legend), wind barbs (one full barb is 5 m s^{-1}, one half barb is 2.5 m s^{-1}, and one flag is 25 m s^{-1}), and geopotential height (contoured) at (a) 1500 UTC 31 Dec and (b) 1800 UTC 27 Feb. The 850-hPa mixing ratio (shaded as in legend), wind barbs (plotted as above), and sea level pressure (hPa; contoured) at (c) as in (a) and (d) as in (b). The storm total precipitation from the (e) Dec and (f) Feb cases.

The maximum rain rate was 9.14 mm h^{-1} at 1800 UTC 27 February. The accumulated precipitation for this time period and stations was 120 mm.

Figures 3c,d show wind profiler data from Sloughhouse, California (see Fig. 1b for location). Note that at the times of maximum rain rate (0900 UTC 31 December and 1500 UTC 31 December for the December case and 1800 UTC 27 February for the February case), there were strong southerly winds at a height of about 500 m with speeds as high as 55 kt for the December

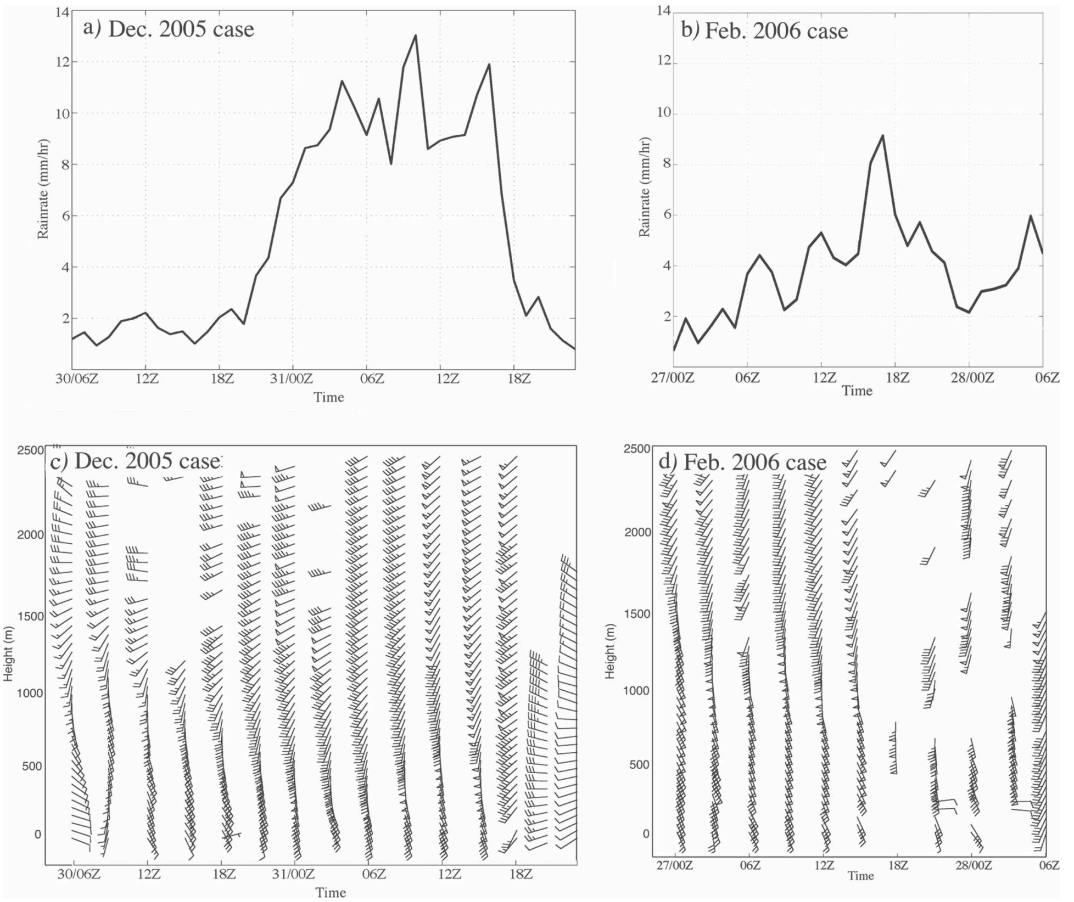

FIG. 3. The averaged hourly rain rate for the highlighted stations shown in Fig. 1c for (a) December and (b) February. The wind profiler measurements (wind barbs plotted as in Fig. 2) at Sloughhouse (see Fig. 1b for location) for (c) December and (d) February.

case and as high as 75 kt for the February case. These wind speed maxima may indicate that a barrier jet was present in both cases. It is plausible that forced ascent of this southerly flow over the southwest facing slope at PNF was responsible for the maximum in precipitation there. This effect of terrain, as well as others, will be explored in the following sections.

3. Numerical simulations

a. Numerical setup

The numerical simulations were performed using the fifth-generation Pennsylvania State University–National Center for Atmospheric Research (PSU–NCAR) Mesoscale Model (MM5, version 3.6; Dudhia 1993; Grell et al. 1994). This mesoscale model is nonhydrostatic and based on terrain-following sigma (σ) vertical coordinates. Two nested domains, with one-way interaction, were used for the simulations (Fig. 4). Domain 1 used 24-km grid spacing with 150 × 175 grid points in the horizontal and a terrain resolution of 19 km. Domain 2 used an 8-km grid spacing with 202 × 196 grid points and a 4-km terrain resolution. Forty-five unevenly spaced, full-sigma levels were used in the vertical with the maximum resolution in the boundary layer. The time steps for domains 1 and 2 were 40 and 15 s, respectively. The NARR was used to initialize the model and update the boundary conditions every 3 h. The Grell (1993) scheme was chosen for cumulus parameterization, Reisner et al. (1998) was chosen for microphysical parameterization, and the Medium-Range Forecast (MRF; Hong and Pan 1996) scheme was selected for the boundary layer parameterization.

The dCTRL simulation (the 30–31 December 2005 case) was initialized at 0000 UTC 30 December and integrated until 0000 UTC 01 January and the fCTRL simulation (the 26–27 February case) was initialized at 2100 UTC 26 February and integrated until 1200 UTC 27 February.

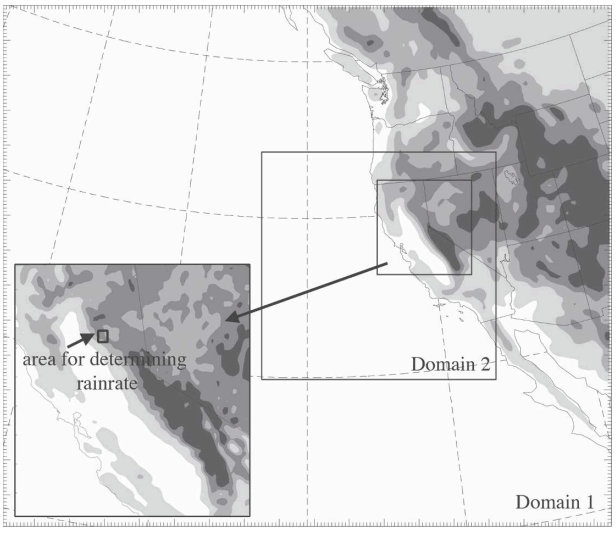

FIG. 4. Model domains used in simulations. The panel inset shows the display domain for Figs. 5e,f, 6e,f, 8, 9, 10, and 11b, and the area over which rain rate was calculated in all simulations.

b. Model verification

At 300 hPa in the dCTRL simulation (Fig. 5a), there was nearly zonal flow incident to and over California. In the fCTRL simulation (Fig. 5b), there was a shortwave trough with a cutoff low positioned just west of the California–Oregon border. At 850 hPa in the dCTRL simulation (Fig. 5c), the flow incident to California was from the west-southwest. A narrow band of enhanced mixing ratios stretched from the west-southwest to the east-northeast. In the fCTRL simulation (Fig. 5d), there was a deep pressure trough oriented in a nearly north–south fashion just off the western U.S. coastline. A cold front symbol has been added to Fig. 5d to indicate that this trough was accompanied by a distinct wind shift, as can be discerned from the 850-hPa wind barbs, and temperature field (not shown). The flow incident to California was from the south–southwest. A well-defined moist tongue was advected toward California, in advance of the baroclinic zone. Comparison of the modeled 300- and 850-hPa flow fields to the observations (Figs. 2a–d) shows very good agreement. The total accumulated precipitation for the dCTRL and fCTRL simulations is shown in Figs. 5e,f, respectively. These analyses also show good agreement with the observations (Figs. 2e,f) with maxima at PNF and elevated accumulations along the coast for both cases. In both simulations, the southwest faces of individual peaks and promontories in the terrain were characterized by enhanced accumulations leading to a cellular structure similar to that noted in Grubišić et al. (2005). However, the greatest accumulations were at PNF.

The rain rate at PNF (which was calculated by averaging the rain rate at all grid points in the back box shown in the inset of Fig. 4) for the dCTRL and fCTRL simulations is shown in Figs. 6a,b, respectively. This area was chosen because it completely encloses the modeled precipitation maximum at PNF in both the dCTRL and fCTRL simulations. In the dCTRL simulation (Fig. 6a), the storm lasted from 1200 UTC 30 December to 1800 UTC 31 December. The maximum rain rate of 15 mm h^{-1} occurred at 1600 UTC 31 December after which the rain rates abruptly decreased. The accumulated precipitation was 284 mm, which is larger than the observations (224 mm). However, we note that rain gauge measurements have been shown to underestimate actual accumulations by between 5% and 25% (Groisman and Legates 1994). The difference in storm total precipitation between the dCTRL simulation and the observed accumulations is within this range. In the fCTRL simulation (Fig. 6b), there was a maximum of 8.1 mm h^{-1} at 1400 UTC 27 February. This maximum occurred 3 h earlier and was slightly smaller than the maximum rain rate from the rain gauge observations. However, the general trend of precipitation was reasonably well captured and the storm total precipitation shows quite good agreement (132 mm for the fCTRL simulation as compared to 120 mm for the observations).

Modeled vertical profiles of wind vectors at Sloughhouse are shown for the dCTRL and fCTRL simulations in Figs. 6c,d, respectively. Between 1200 UTC 31 December and 1800 UTC 31 December for the dCTRL simulation, there was a wind maximum (between 45 and 55 kts) between 500 and 1000 m above ground level (AGL). In the fCTRL simulation, there was a wind maximum of 50 kts at 1200 UTC 27 February and a height of about 1000 m. Although these modeled wind profiles are not identical to the observations (Figs. 4c,d), the presence of a low-level wind maximum in either simulation is indicative of barrier jet formation.

An additional perspective of the mesoscale wind field is provided in Figs. 6e,f, which show the 500-m AGL winds and q at 1600 UTC 31 December for the dCTRL simulation and at 1400 UTC 27 February for the fCTRL simulation, respectively. In both cases, there was southeasterly flow that was moving essentially parallel to the Sierra Nevada mountains in the southern Central Valley.

In the dCTRL simulation, winds entering the Central Valley through the Carquinez Strait exceeded 25 m s^{-1} and moved toward PNF in a near-perpendicular fashion. (Note that the zone of enhanced wind speeds incident to PNF appears to be less related to barrier jet formation than to the onshore movement of a larger-

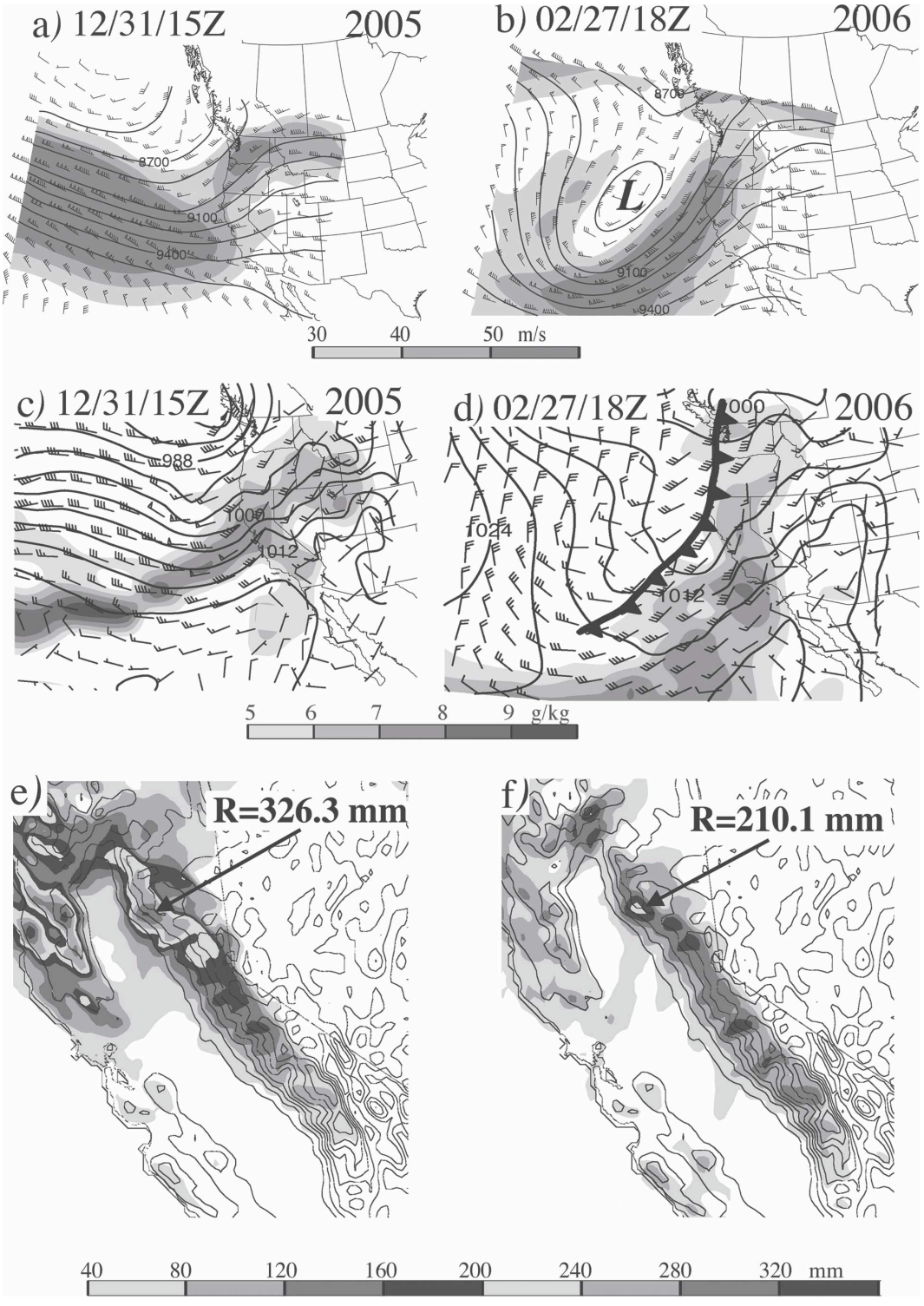

FIG. 5. The 300-hPa wind speeds (shaded as in legend), wind barbs (plotted as in Fig. 2), and geopotential height (m; contoured) for the (a) dCTRL and (b) fCTRL simulations. The 850-hPa wind barbs (plotted as in Fig. 2), mixing ratio (shaded as in legend), and sea level pressure (hPa; contoured) for the (c) dCTRL and (d) fCTRL simulations. The total accumulated precipitation for the (e) dCTRL and (f) fCTRL simulations. The maximum accumulated rain is given for each case.

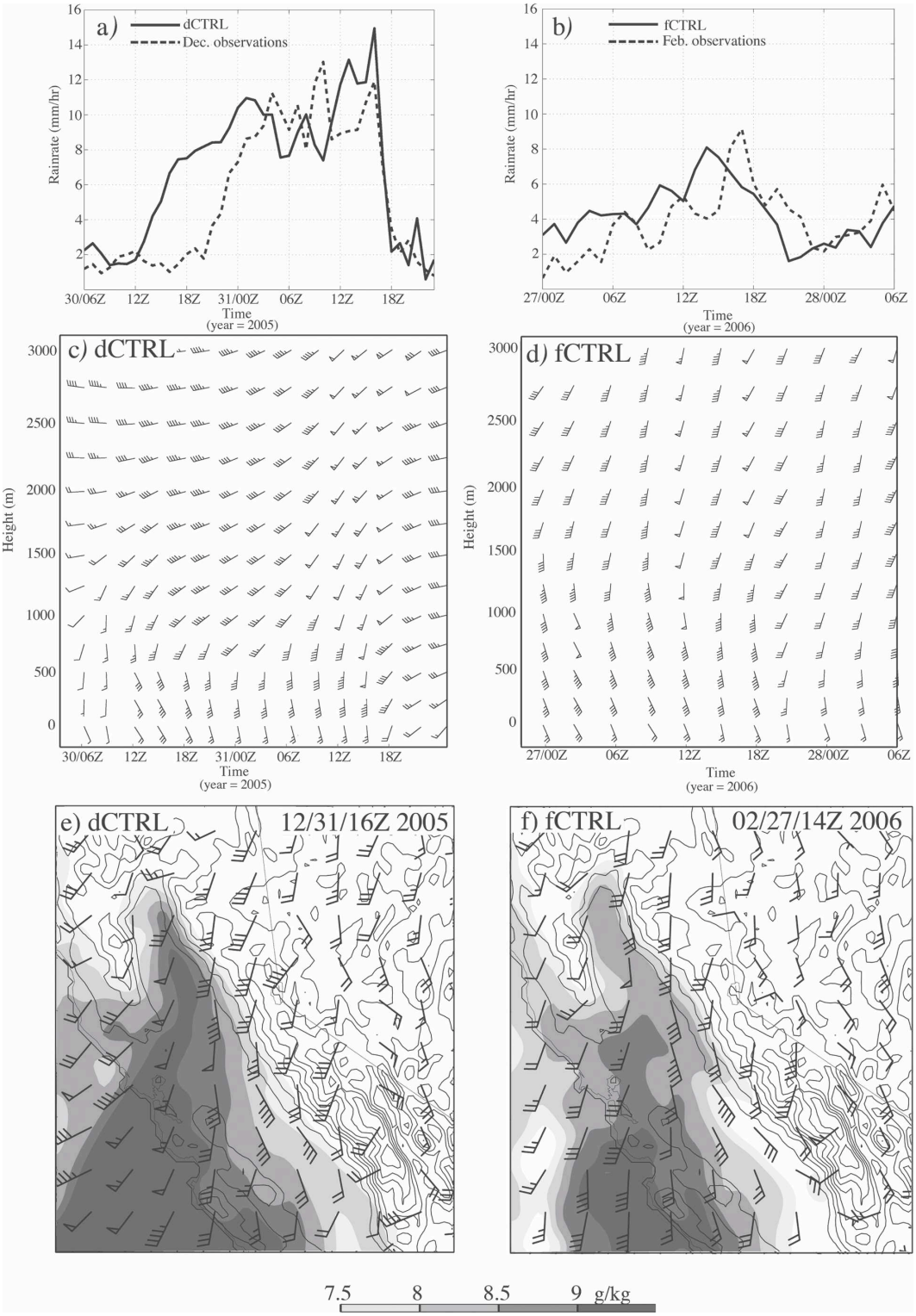

FIG. 6. The averaged hourly rain rate (see Fig. 4 for location) for the (a) dCTRL and (b) fCTRL simulations. The vertical wind profile (wind barbs plotted as in Fig. 2) at Sloughhouse (see Fig. 1b for location) for the (c) dCTRL and (d) fCTRL simulations. The 500-m AGL wind barbs (plotted as in Fig. 2), mixing ratio (shaded as in legend), and terrain (contoured every 400 m) for the (e) dCTRL simulation at 1600 UTC 31 Dec and (f) fCTRL simulation at 1400 UTC 27 Feb.

scale, low-level jet.) In the fCTRL simulation, there was a narrow zone of accelerated winds with speeds as high as 25 m s^{-1} couched against the western face of and moving parallel to the Sierra Nevada mountains. At PNF, the wind traveled upslope rather than alongslope. [This flow pattern is more consistent with known cases of barrier jet formation (Parish 1982; Marwitz 1983, 1987).]

According to linear theory, vertical velocity (w) and, consequently, rain rate are proportional to $U \sin\alpha \partial h/\partial x$, where U is the basic-state wind speed, α is the angle of incidence (as shown in Fig. 7), and $\partial h/\partial x$ is the mountain slope. A decrease in the approach angle of an airstream effectively decreases w, which may, in turn, decrease rain rate. Hence, the enhanced precipitation at PNF may be related to the long-wavelength terrain undulations noted in Fig. 1b since it is at this location that the airstreams approached the terrain with a larger α, as is demonstrated in the conceptual diagram of Fig. 7.

In both the dCTRL and fCTRL cases, relatively moist air ($q > 8.5$ g kg^{-1}) was advected through the Carquinez Strait toward PNF (Figs. 6e,f). Moisture depletion due to precipitation along the upstream side of the Coastal Range appears to have led to decreased moisture advection in the southeast Central Valley. Analyses similar to Figs. 6e,f at earlier and later times (not shown) reveal that the low-level jet and moisture tongue in the dCTRL case experienced a southward drift with time and that the maximum precipitation occurred as the jet's core was centered over the Carquinez Strait. The moist airstream in the fCTRL simulation was more stationary. It is tempting to conclude that the isolated precipitation maximum at PNF was at least partially due to a lack of moisture depletion experienced by airstreams entering the Central Valley through the Carquinez Strait.

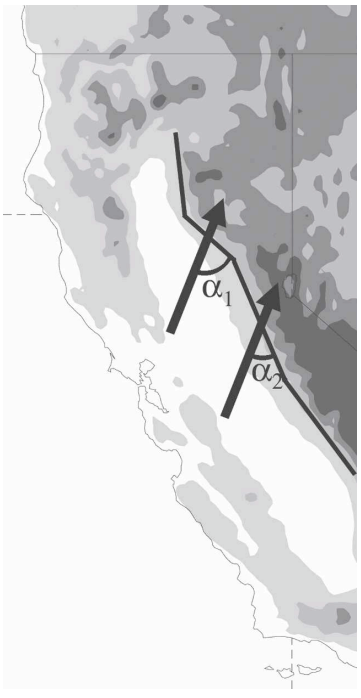

FIG. 7. Conceptual diagram showing wind vectors (thick arrows), angle of incidence (α), and terrain height (shaded as in Fig. 1b).

4. Terrain effects

a. Effects of combined terrain variations

We first attempt to answer the question: Is the precipitation distribution in either the dCTRL or fCTRL simulation dependent on terrain variations particular to the Sierra Nevada mountains? To answer this question, a set of simulations was performed identical to the CTRL simulations except with the terrain replaced by a simple west-southwest facing plateau (see Fig. 8a). These simulations are referred to as the PLATeau or PLAT simulations. Figures 8a,b show the total accumulated precipitation for the December PLAT, or dPLAT, and February PLAT, or fPLAT, simulations, respectively. For the sake of comparison, the location of maximum precipitation in the dCTRL and fCTRL simulations is indicated in Figs. 8a,b by the thick arrow. In both the dPLAT and fPLAT simulations, the precipitation maximum was reduced by about 40 mm for the December case and about 70 mm for the February case as compared to the dCTRL and fCTRL simulations. In the case of the dPLAT simulation, the maximum was shifted slightly to the north of that in the dCTRL simulation. However, the dPLAT simulation did still have an isolated maximum near PNF. This suggests that processes independent of the mesoscale terrain variations are responsible for some degree of localizing the precipitation at PNF, at least for the December case. The accumulated precipitation in the fPLAT simulation showed a very strong sensitivity to the terrain variations. Note that the precipitation distribution in the fPLAT case was fairly evenly distributed with a more-or-less two-dimensional maximum positioned along the mountain slope. (A higher-resolution contouring scheme provides a similar result.)

Figures 8c,d show the 500-m AGL winds and w for the dPLAT and fPLAT simulations at 1600 UTC 31 December and 1400 UTC 27 February, respectively. In the dPLAT simulation, there was a maximum in w of 0.89 m s^{-1} at the location where the southerly deflected winds converged with the more westerly, nondeflected winds to the north. We stress that the maximum in w was not due to the mechanical lifting of the barrier jet

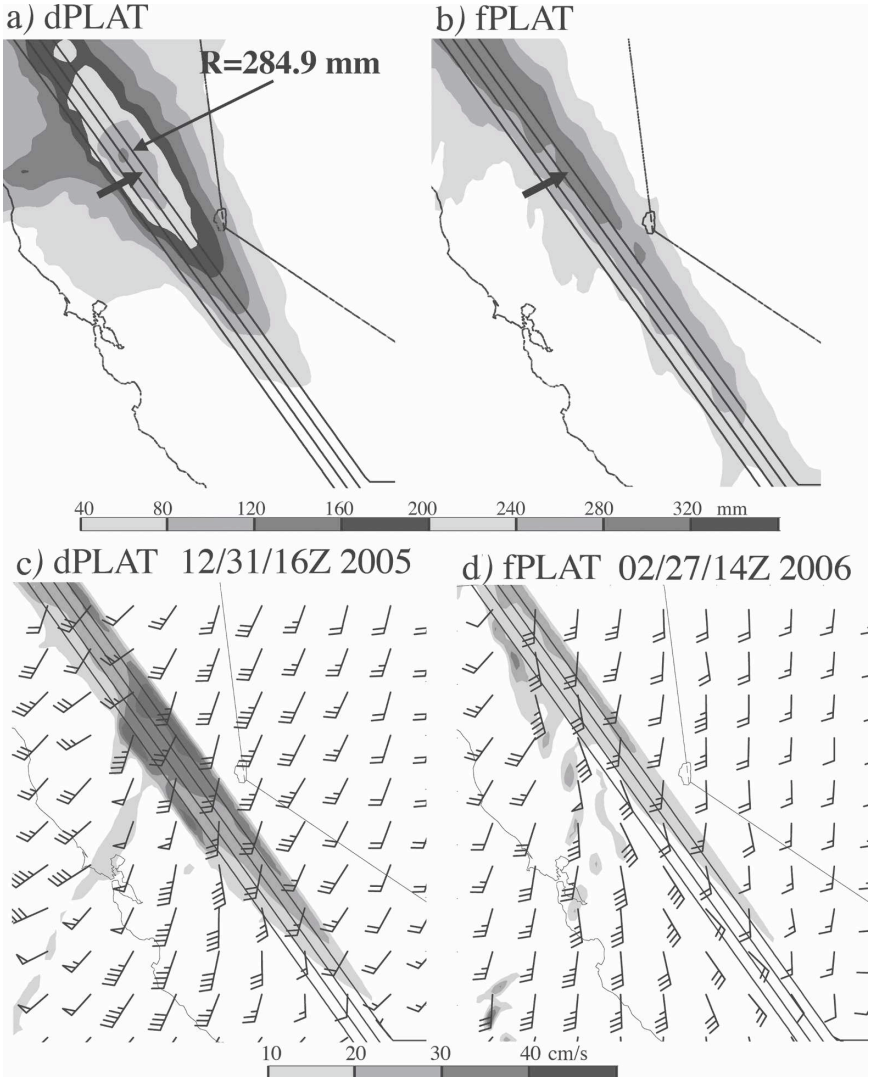

FIG. 8. The total accumulated precipitation (shaded) and terrain height (contoured every 400 m) for the (a) dPLAT and (b) fPLAT simulations. The 500-m AGL winds (plotted as in Fig. 2), vertical velocity (shaded as in legend), and terrain height (thin contours; contoured every 400 m) for the (c) dPLAT simulation at 1600 UTC 31 Dec and the (d) fPLAT simulation at 1400 UTC 27 Feb.

by an uneven terrain slope. In the fPLAT simulation, the convergence and *w* fields were more-or-less two-dimensional and the values for each were fairly conservative.

b. *Effects of the long-wavelength terrain undulations*

The effects of long-wavelength terrain undulations were tested by smoothing out the undulations on the upstream side of the mountains. These simulations, referred to as the No ZigZag (NOZZ; see Fig. 9a) simulations, are otherwise identical to their CTRL counterparts. Note that only the long-wavelength undulations have been removed through smoothing the terrain at lower elevations where they were most pronounced.

The total accumulated precipitation for the December NOZZ, or dNOZZ, and February NOZZ, or fNOZZ, simulations are shown in Figs. 9a,b, respectively. In the dNOZZ simulation, there was an elongated region with precipitation accumulations ranging from 280 to 320 mm. The maximum within this zone was 291.6 mm, which is 34.7 mm less than that in the dCTRL simulation. In the fNOZZ case, the individual maxima were somewhat more elongated, or two-dimensional, as compared to the fCTRL case, and the maximum at PNF was 33.3 mm less than in the fCTRL

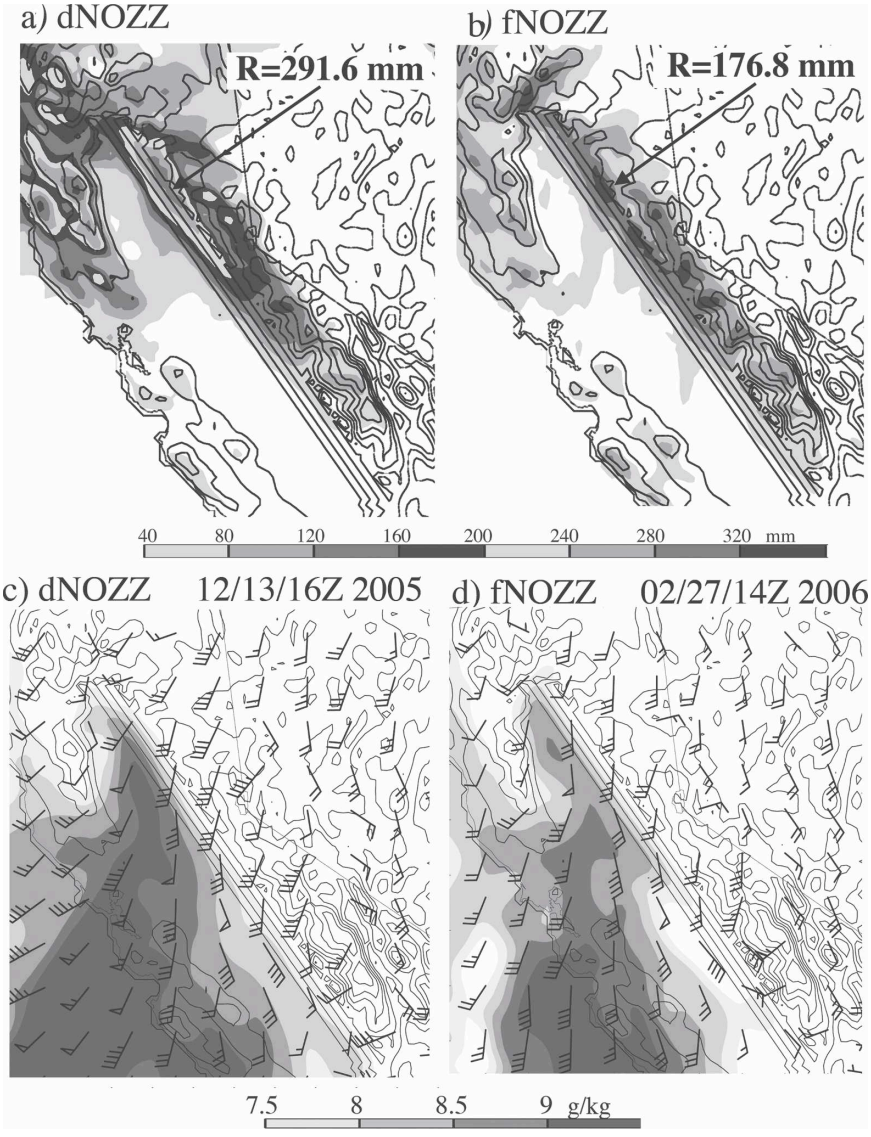

FIG. 9. The total accumulated precipitation (shaded) and terrain height (contoured every 400 m) for the (a) dNOZZ and (b) fNOZZ simulations. The 500-m AGL wind barbs (plotted as in Fig. 2), mixing ratio (shaded as in legend), and terrain height (contoured every 400 m) for the (c) dNOZZ simulation at 1600 UTC 31 Dec and (d) fNOZZ simulation at 1400 UTC 27 Feb.

case. This suggests that the change in slope orientation near PNF was at least partially responsible for enhancing rain rates in both cases.

Figure 9c shows the 500-m AGL winds and q for the dNOZZ simulation at 12/31/16Z. At this time, there was an influx of relatively fast moving (>25 m s^{-1}) moist air ($q > 9$ g kg^{-1}) from offshore and winds in the southern Central Valley were from the southeast. In the fNOZZ simulation (Fig. 9d), there was a fairly narrow zone of enhanced winds (with a maximum just under 25 m s^{-1}) positioned to the west of the mountain slope. A comparison of Figs. 9c,d with Figs. 6e,f shows generally good agreement as far as wind speed and direction are concerned. In both cases, the flow appears to have been partially diverted to the northwest by the terrain with weakly ascending flow along the slope north of Sloughhouse. This was true for other heights below about 1600 m as well. Hence, it appears that the critical difference in the CTRL and NOZZ simulations is that the angle of incidence at PNF was higher in the CTRL cases than in the NOZZ simulations. In the NOZZ simulations, the angle was reduced between 15°

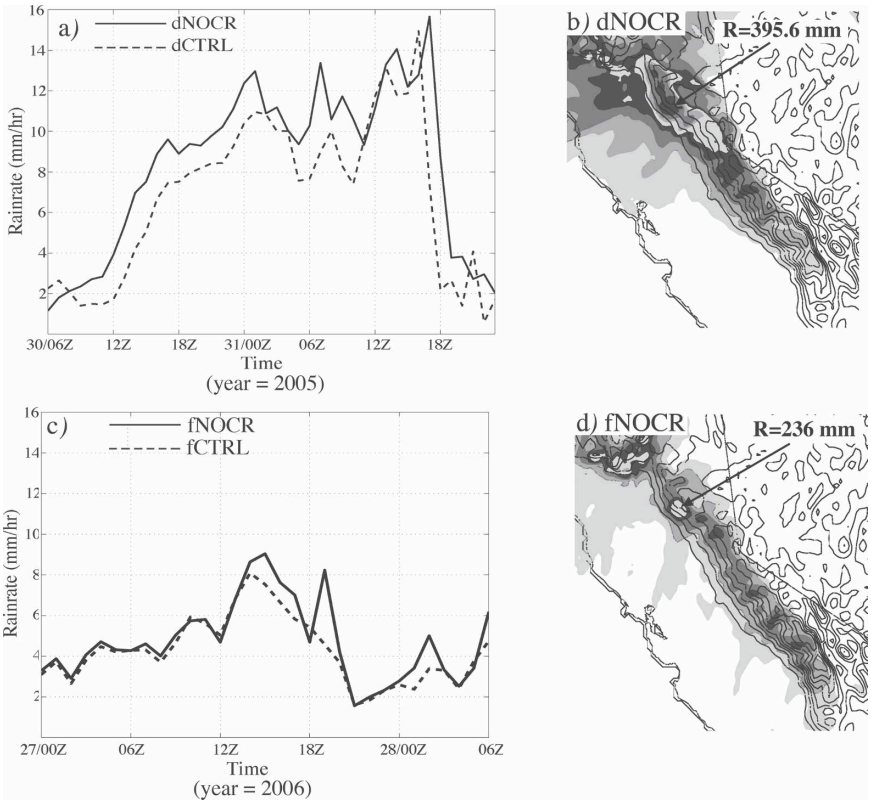

FIG. 10. The hourly rain rate (see Fig. 4 for location) for (a) the dCTRL and dNOCR and (c) fCTRL and fNOCR simulations. The total accumulated precipitation (shaded as in Figs. 9a,b) and terrain height (contoured every 400 m) for the (b) dNOCR and (d) fNOCR simulations. Maximum values of precipitation are given in (b), (d).

and 30°. Consideration of the maximum w at PNF shows that it was reduced from 1.39 to 0.98 m s^{-1} for the December case and from 0.93 to 0.71 m s^{-1} for the February case (not shown) when the terrain undulations were removed.

c. *Effects of the coastal range*

To test the notion that precipitation enhancement at PNF may have been the result of differential moisture depletion along the Coastal Range, a set of simulations identical to the CTRL simulations was performed only with the Coastal Range removed (NOCR simulations). The modified terrain for this simulation is contoured in Fig. 10b.

The primary effect of removing the Coastal Range in the dNOCR simulation was to prolong the amount of time the moisture-bearing low-level jet was able to reach the Sierra Nevada mountains unaffected by upstream orography, as is demonstrated in Fig. 10a, which shows the rain rate at PNF for the dCTRL and dNOCR simulations. The episode of moderate to heavy precipitation (i.e., rain rates >2.08 mm h^{-1}) started roughly 3 h earlier and ended about 2 h later in the dNOCR simulation than in the dCTRL simulation. Individual maxima were also between 2 and 4 mm h^{-1} larger in the NOCR case. The total accumulated precipitation for this case (Fig. 10b) showed a larger maximum at PNF (396.5 mm) than the dCTRL case. However, there was still an isolated maximum at PNF suggesting that some other focusing mechanism was present in this case.

A comparison of the rain rates at PNF for the fNOCR and fCTRL simulations (Fig. 10c) shows that the two simulations agreed quite well as far as the timing of moderate and heavy precipitation onset was concerned. Individual maxima in the rain rates agreed reasonably well. The total accumulated precipitation for the February NOCR, or fNOCR, simulation (Fig. 10d) shows quite good agreement with the fCTRL case (Fig. 5f) with the main exception being that there were noticeably larger accumulations over the southern end of the Sierra Nevada mountains in the fNOCR simulation. The total accumulated precipitation at PNF for the fNOCR case was also somewhat larger than in the fCTRL case (by 25.9 mm). This case showed less sensi-

tivity to the Coastal Range likely because of the quasi-stationary nature of the low-level jet. To briefly summarize, the fCTRL simulation appears to have been very sensitive to the terrain, in particular the short- and long-wavelength undulations, while the dCTRL simulation appears to have had some other mechanism that was relatively independent of small-scale terrain variations acting to enhance rain rates near PNF.

d. *Effect of upstream gradients*

In their investigation of the 1997 New Year's flood, Galewsky and Sobel (2005) argued that the localized maximum present during their case study was the result of upstream gradients in moisture, which led to differential flow blocking along the Sierra Nevada mountains and, therefore, to a localized convergence at PNF. The latter argument is a variant on that used by Rotunno and Ferretti (2001) to explain a similar localized precipitation maximum at Lago Maggiore in the Alps. The argument is based on the fact that orographic blocking depends on the static stability of the air impinging on the mountain and that for saturated flow, this static stability is also a function of low-level moisture content (Durran and Klemp 1982). The effect of moisture-induced, weak static stability was demonstrated by Buzzi et al. (1998), who noted that condensational heating enabled airstreams that would have otherwise been blocked to flow over a mountain barrier. If there exists a sufficiently strong gradient in the upstream moisture content, Rotunno and Ferretti (2001) demonstrated that differential flow blocking may occur where incident airstreams with less moisture are in a flow-around regime, while those with more moisture are in a flow-over regime. Rotunno and Ferretti (2001) demonstrated that the convergence associated with this differential deflection can lead to an isolated precipitation maximum along the mountain slope even if the mountain is two-dimensional and has no small-scale variations. Additionally, their Fig. 10b indicates that the precipitation maximum in their idealized simulations was of a similar spatial scale to that at PNF in the CTRL simulations. It is plausible that such a mechanism could have contributed to the formation of a maximum at PNF for our cases, particularly for the December case whose maximum at PNF seemed to be only dependent on terrain variations in a secondary fashion.

To investigate the effect of large-scale gradients on precipitation, the motion of the so-called heaviest condensating parcel was tracked. This was done by first confirming that the flow incident to PNF was at, or very near to, saturation (not shown). The following formulation was then considered for all pressure layers between the ground and 500 hPa:

$$\Delta C = \int_{z_1}^{z_2} -w \frac{\partial \rho_{vs}}{\partial z}\, dz, \tag{1}$$

where w is the vertical velocity, ρ_{vs} is the saturation vapor density, and ΔC is the condensation rate (Smith 1979). Using model output of density, ρ_{vs}, and w in the boxed area shown in the inset of Fig. 4, ΔC was calculated at the times of maximum rain rate (1600 UTC 31 December for the dCTRL simulation and 1400 UTC 27 February for the fCTRL simulation). The parcel with maximum ΔC according to this formulation was considered to be the heaviest condensator. In the dCTRL simulation, ΔC reached a maximum of 6.04 mm h^{-1} in the 750–725-hPa layer. In the fCTRL simulation, ΔC had a maximum of 2.69 mm h^{-1} in the 750–725-hPa layer.

Figure 11a shows a parcel trajectory for the heaviest condensator in the dCTRL simulation starting at 1600 UTC 31 December and going backward in time to 1000 UTC 31 December. This trajectory is labeled as T3 in Fig. 11a. At 1000 UTC 31 December, T3 was positioned at about 590 km southwest of PNF and at a pressure level of about 950 hPa. It moved in a northeast direction until coming ashore near San Francisco where it experienced a slight northward deflection and ultimately impinged on the mountain at PNF in a near-perpendicular fashion. Forward trajectories originating at T1, T2, T4, and T5 and starting at 1000 UTC 31 December are included in Fig. 11a. Notice that T1, T2, and T3 all converged at PNF. Trajectories 4 and 5 experienced an anticyclonic deflection as they moved toward the Coastal Range, consistent with orographic blocking in the Northern Hemisphere and the partial deflection mechanism of Rotunno and Ferretti (2001). Similar trajectory analyses were performed for the dPLAT and fPLAT simulations and shown in Figs. 11b,c. As noted in Fig. 11a, there was an apparent differential deflection of T1–T5 with the trajectories experiencing greater deflection as one moves southward resulting in confluence at PNF. This relatively large-scale deflection is ultimately responsible for the barrier jets noted in Figs. 6e,f.

Trajectory confluence, although symptomatic of a larger-scale differential deflection, is not sufficient in and of itself to prove that the mechanism was active or that it was instrumental in localizing precipitation at PNF, as a trajectory analysis identical to that in the fPLAT simulation only for a simulation with no terrain (not shown) shows T1–T3 had similar paths to those in Fig. 11c. The distinguishing difference between the December and February cases lies in the cross-stream gradients of moisture and wind speed. Table 1 shows the precipitable water, wind speed, and Brunt–Väisälä fre-

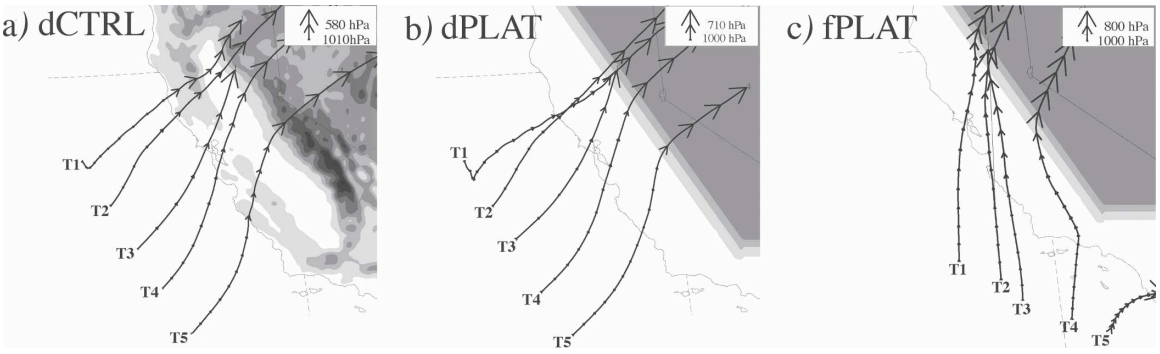

FIG. 11. Trajectory analysis for the (a) dCTRL, (b) dPLAT, and (c) fPLAT simulations In (a), (b), trajectory T3 was started at 1600 UTC 31 Dec 2005 and goes backward in time until 1000 UTC 31 Dec ending at the label for T3; all other trajectories were started at 1000 UTC 31 Dec at the locations marked as T1, T2, T4, and T5 and integrated forward in time until 0000 UTC 1 Jan 2006. In (c), T3 was started at 1400 UTC 27 Feb and integrated backward in time until 0800 UTC 27 Feb ending at the label T3; all other trajectories were started at 0800 UTC 27 Feb at the locations marked as T1, T2, T4, and T5 and integrated forward in time until 0000 UTC 3 Mar. In (a)–(c), terrain height is shaded as in Fig. 1b; each arrow head denotes an interval of 1 h.

quency (N) from 0 to 2000 m at the origins of T1–T5 for the dCTRL and fCTRL simulations (the origins of the trajectories in the fCTRL simulation are identical to those shown for the fPLAT simulation in Fig. 11c). Both cases had weak gradients in N. The dCTRL simulation had a stronger gradient in both precipitable water and wind speed (this is also evident in Figs. 5c,d), consistent with the differential deflection mechanism of Rotunno and Ferretti (2001).

5. Conclusions

Two cases of heavy precipitation along the northern half of the Sierra Nevada mountains have been investigated in an attempt to understand the mechanisms responsible for isolated precipitation maxima located in the vicinity of Plumas National Forest (PNF). The large-scale flow patterns were quite different for each case with the first case (30–31 December 2005) having predominantly zonal flow. The second case (27–28 February 2006) had predominantly meridional flow and strong low-level baroclinicity. Both cases had what appeared to be a strong southerly barrier jet in the observed wind profiler data. Whether the forced ascent of this southerly flow over the southwest facing portion of the Sierra Nevada mountains caused the precipitation maximum near PNF was explored in a series of numerical experiments. Other probable sources of precipitation enhancement at PNF were also examined.

The control (CTRL) simulations of the December and February cases generally captured the observed flows quite well with only minor differences in rain rate and the height of the wind maximum in the February case. Additional analyses of low-level winds show the fCTRL simulation had a barrier jet–like feature that appeared to be forced over the Sierra Nevada mountains where the slope orientation is more southwesterly (i.e., at PNF). The wind maximum in the dCTRL simulation was due to the onshore movement of a larger-scale low-level jet whose flow was nearly perpendicular to the terrain near PNF.

The removal of all terrain features save for the basic plateau (the PLAT simulations) resulted in no isolated precipitation maximum in the February case. However, the December case still had an isolated precipitation maximum near PNF. Smoothing out the long-wavelength undulations along the west face of the Sierra Nevada mountains (the NOZZ simulations) had a similar effect although the contrasts between these simulations and their CTRL counterparts were not as distinct as those between the CTRL simulations and the PLAT simulations. Reduced accumulations at PNF in the NOZZ simulations appear to be due to the decrease in the angle incident airstreams made with the slope near PNF. This decrease was associated with a decrease in the vertical velocity along the mountain slope. The high degree of sensitivity to terrain undulations (both short and high wavelength) in the February case indi-

TABLE 1. The values of precipitable water (pwtr), wind speed (wsp), and Brunt–Väisälä frequency (N) at the origins of trajectories 1–5 (T1–T5) from the dCTRL and fCTRL simulations.

		T1	T2	T3	T4	T5
dCTRL	pwtr (mm)	30.0	32.8	27.3	26.5	23.6
	wsp ($m\ s^{-1}$)	12.0	22.8	20.0	18.5	14.6
	N (s^{-1})	1.39	1.21	1.19	1.28	1.47
fCTRL	pwtr (mm)	26.7	28.7	30.5	29.3	28.6
	wsp ($m\ s^{-1}$)	15.6	15.5	14.1	11.3	7.6
	N (s^{-1})	1.07	1.16	1.17	1.18	1.34

cates that the terrain was instrumental in focusing and enhancing precipitation at PNF. The December case, however, shows much less sensitivity to terrain as far as the precipitation pattern was concerned. This latter result challenges the notion that enhanced precipitation occurs solely as a result of a barrier jet experiencing terrain-forced ascent along the southwest facing slopes at PNF.

The effects of moisture depletion along the upstream sides of the Coastal Range were also tested in a set of simulations where these mountains were removed (the NOCR simulations). The accumulated precipitation at PNF was larger in the NOCR simulations than in the corresponding CTRL simulations but, more importantly, both cases still had an isolated maximum at PNF suggesting that although the Coastal Range does modulate the intensity of precipitation, it does not significantly modulate the pattern of precipitation. Curiously enough, the maximum in the dNOCR simulations was 110.7 mm larger than that in the dPLAT simulation. Intuitively, it seems that the maximum at PNF should have had a similar magnitude in either simulation since neither case was subject to moisture depletion by the Coastal Range. This difference serves to indicate how important small-scale terrain inhomogeneities are for the enhancement of precipitation. Resolution dependency of these results is one area of further research worthy of study.

An alternative explanation for the maximum at PNF in the December case is that differential deflection of incident airstreams to the Sierra Nevada mountains led to localized convergence, vertical velocity, and finally, to enhanced rain rates in the vicinity of PNF. Inspection of parcel trajectories in the dCTRL and dPLAT simulations shows confluence in the vicinity of PNF. Ultimately, this differential deflection appears to have been driven by strong gradients in the upstream moisture distribution. The upstream moisture distribution in the February case was nearly constant, which seems to account for the greater sensitivity to terrain in this case.

The overriding result is that moderate to heavy precipitation events in California are not necessarily driven by the same dynamics. Some cases have flow patterns that are very sensitive to terrain variations (short- and long-wavelength undulations in particular) and some cases are dominated by large upstream gradients in moisture that are ultimately driven by synoptic-scale flow patterns.

Acknowledgments. Special thanks are extended to three anonymous reviewers, D. Kingsmill, R. Smith, PAMS HPC, data archives at UWYO, ESRL, and NCAR. This work was supported by NSF Grant ATM-0344237.

REFERENCES

Buzzi, A., N. Tartaglione, and P. Malguzzi, 1998: Numerical simulations of the 1994 Piedmont flood: Role of orography and moist processes. *Mon. Wea. Rev.,* **126,** 2369–2383.

Colle, B. A., B. F. Smull, and M.-J. Yang, 2002: Numerical simulations of a land-falling cold front observed during COAST: Rapid evolution and responsible mechanisms. *Mon. Wea. Rev.,* **130,** 1945–1966.

Dettinger, M., K. Redmond, and D. Cayan, 2004: Winter orographic precipitation ratios in the Sierra Nevada—Large-scale atmospheric circulations and hydrologic consequences. *J. Hydrometeor.,* **5,** 1102–1116.

Dudhia, J., 1993: A nonhydrostatic version of the Penn State-NCAR mesoscale model: Validation tests and simulation of an Atlantic cyclone and cold front. *Mon. Wea. Rev.,* **121,** 1493–1513.

Durran, D. R., and J. B. Klemp, 1982: On the effects of moisture on the Brunt-Väisälä frequency. *J. Atmos. Sci.,* **39,** 2152–2158.

Galewsky, J., and A. Sobel, 2005: Moist dynamics and orographic precipitation in northern and central California during the New Year's Flood of 1997. *Mon. Wea. Rev.,* **133,** 1594–1612.

Gershunov, A., T. P. Barnett, D. R. Cayan, T. Tubbs, and L. Goddard, 2000: Predicting and downscaling ENSO impacts on intraseasonal precipitation statistics in California: The 1997/98 event. *J. Hydrometeor.,* **1,** 201–210.

Grell, G. A., 1993: Prognostic evaluation of assumptions used by cumulus parameterizations. *Mon. Wea. Rev.,* **121,** 764–787.

——, J. Dudhia, and D. R. Stauffer, 1994: A description of the fifth-generation Penn State/NCAR mesoscale model (MM5). NCAR Tech. Note NCAR/TN-398+STR, 138 pp. [Available from National Center for Atmospheric Research, P.O. Box 3000, Boulder, CO 80307.]

Groisman, P. Y., and D. R. Legates, 1994: The accuracy of United States precipitation data. *Bull. Amer. Meteor. Soc.,* **75,** 215–227.

Grubišić, V., R. K. Vellore, and A. W. Huggins, 2005: Quantitative precipitation forecasting of wintertime storms in the Sierra Nevada: Sensitivity to microphysical parameterization and horizontal resolution. *Mon. Wea. Rev.,* **133,** 2834–2859.

Heggli, M. F., and D. W. Reynolds, 1985: Radiometric observations of supercooled liquid water within a split front over the Sierra Nevada. *J. Climate Appl. Meteor.,* **24,** 1258–1261.

——, and R. M. Rauber, 1988: The characteristics and evolution of supercooled water in wintertime storms over the Sierra Nevada: A summary of microwave radiometric measurements taken during the Sierra Cooperative Pilot Project. *J. Appl. Meteor.,* **27,** 989–1015.

Hong, S.-Y., and H.-L. Pan, 1996: Nonlocal boundary layer vertical diffusion in a medium-range forecast model. *Mon. Wea. Rev.,* **124,** 2322–2339.

James, C. N., and R. A. Houze Jr., 2005: Modification of precipitation by coastal orography in storms crossing Northern California. *Mon. Wea. Rev.,* **133,** 3110–3131.

Kim, J., N. L. Miller, J. D. Farrara, and S.-Y. Hong, 2000: Seasonal precipitation and streamflow hindcast and prediction study in

the western United States during the 1997/98 winter season using a dynamic downscaling system. *J. Hydrometeor.,* **1,** 311–329.

Kingsmill, D. E., P. J. Neiman, F. M. Ralph, and A. B. White, 2006: Synoptic and topographic variability of northern California precipitation characteristics in landfalling winter storms observed during CALJET. *Mon. Wea. Rev.,* **134,** 2072–2094.

Leung, L. R., and Y. Qian, 2003: The sensitivity of precipitation and snowpack simulations to model resolution via nesting in regions of complex terrain. *J. Hydrometeor.,* **4,** 1025–1043.

Marwitz, J. D., 1983: The kinematics of orographic airflow during Sierra storms. *J. Atmos. Sci.,* **40,** 1218–1227.

——, 1987: Deep orographic storms over the Sierra Nevada. Part I: Thermodynamic and kinematic structure. *J. Atmos. Sci.,* **44,** 159–173.

Mesinger, F., and Coauthors, 2006: North American Regional Reanalysis. *Bull. Amer. Meteor. Soc.,* **87,** 343–360.

Meyers, M. P., and W. R. Cotton, 1992: Evaluation of the potential for wintertime quantitative precipitation forecasting over mountainous terrain with an explicit cloud model. Part I: Two-dimensional sensitivity experiments. *J. Appl. Meteor.,* **31,** 26–50.

Miller, N. L., and J. Kim, 1996: Numerical prediction of precipitation and river flow over the Russian River watershed during the January 1995 California storms. *Bull. Amer. Meteor. Soc.,* **77,** 101–105.

Mitchell, T. P., and W. Blier, 1997: The variability of wintertime precipitation in the region of California. *J. Climate,* **10,** 2261–2276.

Mo, K. C., J.-K. Schemm, H. M. H. Juang, R. W. Higgins, and Y. Song, 2005: Impact of model resolution on the prediction of summer precipitation over the United States and Mexico. *J. Climate,* **18,** 3910–3927.

Neiman, P. J., P. O. G. Persson, F. M. Ralph, D. P. Jorgensen, A. B. White, and D. E. Kingsmill, 2004: Modification of fronts and precipitation by coastal blocking during an intense landfalling winter storm in southern California: Observations during CALJET. *Mon. Wea. Rev.,* **132,** 242–273.

Pandey, G. R., D. R. Cayan, M. D. Dettinger, and K. P. Georgakakos, 2000: A hybrid orographic plus statistical model for downscaling daily precipitation in northern California. *J. Hydrometeor.,* **1,** 491–506.

Parish, T. R., 1982: Barrier winds along the Sierra Nevada mountains. *J. Appl. Meteor.,* **21,** 925–930.

Persson, P. O. G., P. J. Neiman, B. Walter, J.-W. Bao, and F. M. Ralph, 2005: Contributions from California coastal-zone surface fluxes to heavy coastal precipitation: A CALJET case study during the strong El Niño of 1998. *Mon. Wea. Rev.,* **133,** 1175–1198.

Ralph, F. M., P. J. Neiman, and G. A. Wick, 2004: Satellite and CALJET aircraft observations of atmospheric rivers over the eastern north Pacific Ocean during the winter of 1997/98. *Mon. Wea. Rev.,* **132,** 1721–1745.

——, ——, and R. Rotunno, 2005: Dropsonde observations in low-level jets over the northeastern Pacific ocean from CALJET-1998 and PACJET-2001: Mean vertical-profile and atmospheric-river characteristics. *Mon. Wea. Rev.,* **133,** 889–910.

Rauber, R. M., 1992: Microphysical structure and evolution of a central Sierra Nevada orographic cloud system. *J. Appl. Meteor.,* **31,** 3–24.

Reisner, J., R. Rasmussen, and R. T. Bruintjes, 1998: Explicit forecasting of supercooled liquid water in winter storms using the MM5 mesoscale model. *Quart. J. Roy. Meteor. Soc.,* **124,** 1071–1107.

Reynolds, D. W., and A. P. Kuciauskas, 1988: Remote and in situ observations of Sierra Nevada winter mountain clouds: Relationships between mesoscale structure, precipitation and liquid water. *J. Appl. Meteor.,* **27,** 140–156.

Rogers, E., D. G. Deaven, and G. S. Dimego, 1995: The regional analysis system for the operational "early" Eta model: Original 80-km configuration and recent changes. *Wea. Forecasting,* **10,** 810–825.

Rotunno, R., and R. Ferretti, 2001: Mechanisms of intense Alpine rainfall. *J. Atmos. Sci.,* **58,** 1732–1749.

Smith, R. B., 1979: The influence of mountains on the atmosphere. *Adv. Geophys.,* **21,** 87–230.

White, A. B., P. J. Neiman, F. M. Ralph, D. E. Kingsmill, and P. O. G. Persson, 2003: Coastal orographic rainfall processes observed by radar during the California land-falling jets experiment. *J. Hydrometeor.,* **4,** 264–282.

Yu, C.-K., and B. F. Smull, 2000: Airborne Doppler observations of a landfalling cold front upstream of steep coastal orography. *Mon. Wea. Rev.,* **128,** 1577–1603.

Yuan, H., S. L. Mullen, X. Gao, S. Sorooshian, J. Du, and H.-M. H. Juang, 2005: Verification of probabilistic quantitative precipitation forecasts over the southwest United States during winter 2002/03 by the RSM ensemble system. *Mon. Wea. Rev.,* **133,** 279–294.